Multilayer Methylcellulose Substrate-Based Wearable Touch Sensor and Display for Communication

Kim Yunsu
Inha University
Sung-pil Chang
Inha University
Youngjun Song (✉ yjunsong@inu.ac.kr)
Incheon National University

Research Article

Keywords: Cellulose substrate, Composite, Flexible printed circuit board, Light-emitting diode display, Touch panel

Posted Date: November 19th, 2021

DOI: https://doi.org/10.21203/rs.3.rs-1015537/v1

Abstract

In recent years, flexible printed circuit boards (FPCBs) that have polyimide substrates have been widely used in electronic devices for industrial and academic research owing to their light weight, high dielectric constant, and flexibility. However, these FPCBs have a critical limitation of recycling, as polyimide is not degradable or eco-friendly. To overcome this issue, we fabricated cellulose-based FPCBs. Transparent and flexible methyl cellulose-based substrate was produced through a simple solvent evaporation process. The circuit layer was patterned of an Ag/carbon-nanotube composite fabricated using a stencil mask. The methyl cellulose-based FPCBs were evaluated for diverse mechanical stresses such as bending, torsional, and tensile stresses. In addition, their surface morphology was analyzed using optical microscopy and scanning electron microscopy. For the electrical properties, in addition to the current–voltage curves, their dielectric properties were analyzed. Finally, we reported the successful wearable communication device of the cellulose-based FPCBs in a 5 × 5 touch panel and a 5 × 5 light-emitting diode display.

Introduction

Cellulose-based substrates in electronic devices have been the focus of various circuit applications owing to their nontoxic and environmentally friendly nature (Steckl 2013; Alimenti et al. 2015; Jung et al. 2015). Paper electronics based on cellulose have various benefits such as disposability, low cost, easy handling, and degradability. For example, the conductive ink circuits on a standard copy paper, which have foldability and flexibility, provide craft and origami with electrical properties (Shin et al. 2016). In addition, paper electronics have demonstrated their use in various applications, including supercapacitors, rechargeable batteries, sensors and actuators, diagnostic devices, and microfluidic systems (Ko et al. 2017; Jabbour et. al 2013; Guan et al. 2021; Wang et al. 2014; Shin and Hyun 2017). In recent years, focus has been on cellulose substrates owing to their unique property of optical transparency via their nanostructures (Fujisaki et al. 2014; Nogi et al. 2009). Transparent substrates made of cellulose nanofibers with TEMPO-oxidation and of crystalline cellulose are fabricated by hot pressing similar to the paper fabrication process. (Wang et al. 2013) However, other transparent cellulose-based substrates, such as methyl cellulose (MC) and nitrocellulose (NC), are fabricated by the solvent evaporation process (Song et al. 2017; Noh et al. 2021).

These transparent cellulose-based substrates have been investigated for diverse applications, such as flexible and transparent electrodes, solar cells, and organic transistors. (Koga et al. 2014; Ebner et al. 2017; Dai et al. 2018) Owing to their thin polymer film structure and the percolation network of conductive nanomaterials (carbon nanotubes (CNTs), Ag nanowires (NWs), CuNWs, and conductive polymers), these substrates exhibit flexibility along with conductivity and transparency (Nair et al. 2015; Han et al. 2014). Polymer solar cells on transparent cellulose-based substrates show increased quantum yields because of the increased haze of the substrates (Ham et al. 2016). A flexible and transparent transistor has been fabricated using CNTs and a conductive polymer. Moreover, the mechanical properties of cellulose-based

substrates makes them easy to handle for tasks such as cutting, bending, and folding (Nagashima et al. 2014).

In industries and academic research, the flexibility of an electronic circuit has a significant role in applications such as bending smartphones and wearable devices (Park et al. 2014; Son et al. 2014). Polyimide (PI) substrates are widely used for fabricating flexible printed circuit boards (FPCBs) (Kamiya et al. 2007). FPCBs are being broadly developed for wearable devices capable of sensing body signals to perform electrocardiography and electromyography (Kim et al. 2008; Yeon et al. 2020). Furthermore, the flexibility of an FPCB provides stable electrical performance for soft robots (Lee et al. 2017). Currently, the high-resolution patterning of FPCBs is being performed via photolithography for the fabrication of FPCBs for these advanced applications (Chu et al. 2019). This fabrication process provides an advanced minimum feature size of the FPCBs (Lee et al. 2020). This allows the fabrication of multilayer circuits of other substrates, which are electrically connected to the bottom layer with via holes.

For FPCBs, cellulose-based substrates have several beneficial properties. (1) They have a fabrication process similar to that of FPCB circuitry patterning. (2) They can be appiled to easily fabricate multilayer circuits. (3) They have a high dielectric constant. (4) Their thin films are flexible. (5) Their devices are disposable owing to the biodegradability of cellulose. (6) Their films fabricated by hot pressing or solvent evaporation are transparent. (7) They are nontoxic.

In this study, we report the fabrication of a wearable touch panel and display array based on multilayer MC substrates. The material properties of the MC substrate were investigated using X-ray diffraction (XRD) and Fourier transform infrared spectroscopy (FTIR). The mechanical stability of the substrates was investigated by measuring the stress–strain curves and resistance ratio (R/R_0) with respect to strain. Furthermore, the dielectric constants of the MC substrates with different thicknesses were evaluated from their capacitances. To analyze the electrical performance of the substrates with Ag/CNT composite circuits under mechanical stresses, the current–voltage (I–V) curves and resistance ratio with respect to bending and torsional stresses were measured. The Ag/CNT circuitry was patterned onto the substrates using a shadow mask, and the LEDs were implanted on the circuit pattern. The LED circuit pattern was extended to a 5 × 5 LED array, which could operate to display an English letter. In order to fabricate the wearable devices, a 5 × 5 ring Ag/CNT circuit pattern on an MC hole cover layer was layered onto another 5 × 5 Ag/CNT circuit pattern. The wearable device consisted of a touch capacitance sensor panel, which was worn around a human wrist. Using a small via hole on the MC layer, the multilayer LED circuit was fabricated and then analyzed by Scanning electron microscopy (SEM). The via hole layer was aligned with the Ag/CNT composite circuit pattern to fabricate the multilayer 5 × 5 LED array. Finally, the touch panel and LED display were connected using a microprocessor and personal computer system.

Methods

Materials and preparation

MC powder (4–12% hydroxypropyl) and dimethyl sulfoxide (DMSO) were purchased from Sigma-Aldrich (USA). For a 20 wt.% suspension, MC and DMSO were mixed in the ratio 1:5, respectively, and sonicated for 1 h in a Powersonic 510 sonicator (Hwashin Tech, South Korea). The solubility of MC in various suspensions was monitored using diverse solvents, such as 99% grade EtOH (Sigma-Aldrich, USA) and isopropyl alcohol (IPA, ACS Material, USA)), through the solvent mixing process. After the suspensions were poured into flat Petri dishes (4science, South Korea) of diameter 70 mm, the samples were dried on an MS300HS hotplate (iNtRON Biotechnology, South Korea) at 85°C for 24 h. After the samples were completely dried, they were shifted from the Petri dishes to the lab desk and maintained at room temperature for 1 h. For the electric circuits, the Ag/CNT composites were composed of Elcoat P-100 Ag conductive ink (Cans Co., USA) and CNTs of diameter 7–15 nm and length 0.5–10 μm (Sigma-Aldrich, USA). Ag and CNTs were mixed together in a 20:1 ratio in IPA and sonicated for 1 h. Then, the composite solutions were dried on a hotplate at 85°C for 30 min.

Characterization

The thicknesses of the MC substrates were measured using a BD500-300 digital caliper (Blue Tec, USA). The stress–strain curves of the substrates with varying thicknesses were measured using a tensile strength tester (Hand PI instrument, China). The resistances of the conductive material on the substrates were measured using a Keithley 2450 source meter (Keithley Instruments, USA), and the I-V curves were measured using the Keithley 2450 source meter with a custom software. The capacitances of the substrates were measured using an Agilent E4980A LCR meter (Keysight, USA). FTIR was performed using a Vertex 80v vacuum FTIR (Bruker, USA) and a Hyperion 2000 FTIR microscope (Bruker, USA). The XRD patterns were measured by HR-XRD (Smart Lab, Rigaku, USA) using Kα Cu radiations from 10° to 90° at 45 kV/200 mA. The SEM images of the surface morphology of the substrates were obtained using an AIS2500C at 10 kV (Seron Technology Inc, South Korea).

Circuit Fabrication

Red, orange, and blue surface mount device (SMD) type light-emitting diode (LED) components were purchased from Device Mart (South Korea). The circuit pattern was designed using AutoCAD 2020 (Autodesk, USA). For the shadow mask, a polyethylene terephthalate (PET) film (4science, South Korea) was cut using L3020 laser cutters (Rexbot, South Korea). For the circuits, the Ag/CNT composite was deposited onto the MC substrates using the PET mask. To enhance the pattern resolution, the mask was attached to the substrate using a double-sided tape (3M, USA). After the PET mask was removed from the substrate, the Ag/CNT composite was cured for 1 h at room temperature. The SMD LEDs were assembled on the circuit pattern.

FPCB operation

The MC FPCB was connected to the Uno Arduino development board system (Arduino, Italy) and the development board was connected to a Microsoft foundation class (MFC visual C++). The MFC visual C++ was configured as the MC FPCB's control and display. A customized program was developed to control the FPCB, as shown in Figure S4.

Result

The fabrication process of transparent MC FPCB

Wearable and deformed electronic devices consisting of FPCBs that are based on polyimide (PI) are widely used in industries and academic research. Although PI has advantages, such as mechanical strength, high dielectric constant, and flexibility, it is not an environmentally friendly material. To overcome this limitation, cellulose, which is found in wood and plants, has been used to replace PI as an FPCB substrate (Kim et al. 2006). Figure 1 shows the fabrication process and images of the flexible circuits with MC substrates. In MC, 27–32% of the hydroxyl groups exist in the form of methoxy (Gustafsson et al. 1999) and thus MC dissolved in the aprotic polar solvent DMSO. Owing to the degree of substitution (DOS), MC was insoluble in the other solvents such as ethanol and alcohol as shown in Figure S1. Figure 1 (a) shows a schematic of the fabrication process of the MC substrates. First, 2% w/v of MC in DMSO was sonicated for 1 h to increase its solubility. The MC suspension was poured into a Petri dish and DMSO was evaporated at 85°C for 24 h using a hotplate. The evaporation of DMSO caused the completely dissolved MC (2% w/v) to change from a transparent gel state to a thin film state (Figure 1 (b)). For controlling the thickness, the flat MC substrates were fabricated in the Petri dishes of diameter 70 mm using the amounts of suspension as shown in Figure S2. By the dissolution in DMSO and the subsequent evaporation of DMSO, transparent and non-porous MC substrates for flexible electronic devices were fabricated. Their surface morphology was determined using SEM (Figure 1 (c)). The thin and flexible MC substrate could be used as an electronic circuit substrate in wearable devices or flexible displays. To improve the mechanical endurance of the circuits, high aspect ratio CNTs were used for the Ag/CNT composites. The composite suspensions, which had various concentrations of Ag and CNTs in IPA, were sonicated for 1 h. Then, their viscosities were increased by heating them at 85°C for 30 min. The Ag/CNT composite circuits were deposited onto the MC substrates via stencil masks. Then, the circuits were completely dried at room temperature for 30 min. Figure 1 (d) shows the fabrication of the circuit onto a MC substrate without the LED implantation. Figures 1 (e) and (f) show a parallel LED circuit on an MC substrate in operation. Figures (g–i) show single layer and multilayer Ag/CNT circuits on MC substrates. Single layer and multilayer Ag/CNT composite circuits with thin-film MC substrates can be used in various applications such as LED circuits, touch panels, and active and passive matrix LED displays.

Characteristics of MC substrate

The XRD pattern of the MC substrate is shown in Figure 2 (a). The diffraction curve exhibited high intensity peaks at 2θ values of approximately 13.4° and 20°; the strongest peak was at 20°. The FTIR spectrum of the MC substrate is shown in Figure 2 (b). The absorption band showed a peak at approximately 3451 cm^{-1} of the O-H stretching vibration and a peak at approximately 2921 cm^{-1} owing to the asymmetric stretching vibration due to C-H stretching. The strong peak formed at 1455 cm^{-1} indicated the presence of a benzene ring. The peak at 1315 cm^{-1} was attributed to the C-H bending

vibration. The peaks at 1100–1150 cm^{-1} and 944.93 cm^{-1} were attributed to the C-O stretching vibration and C-O stretching, respectively.

Stress–strain curves of the MC substrate

An FPCB should be robust in order to maintain a stable electrical performance under an external mechanical force. Figure 3 shows the force-strain curves and resistance ratios with respect to strain of the MC substrates with various thicknesses. The stress–strain curves of the 7.5 × 2.5 mm MC substrates were measured until they underwent failure as shown in Figure 3 (a). All MC substrates, which had thicknesses of 100 μm, 200 μm, and 300 μm, underwent failure at a strain of 0.266 mm/mm. However, the force exerted on the MC substrates with thicknesses of 100 μm, 200 μm, and 300 μm at a strain of 0.10 mm/mm was 20 N, 40 N, and 100 N, respectively. It was observed that the mechanical endurance of the MC substrates increased with thickness, as the elongation rate significantly reduced as the gauge length/width ratio increased, according to Yu et al. (2004); Kumar et. al (2016). In addition, the ductility and Young's modulus (1) depended on the gauge length.

$$\sigma_1 = \frac{E \times e_1}{10.03} \qquad (1)$$

where E is the ratio of the longitudinal stress (σ_1) to the longitudinal strain (e_1). All of the MC substrates showed a linear increase in the force with strain for the yield strength of the polymer film (Lim and Hoag 2013). In addition, the slopes of the force-strain curves linearly increased with the thickness of the MC substrates (McKenna et al. 2009).

We measured the resistance ratio (R/R0) with respect to the strain (mm/mm) of the MC substrates with various thicknesses as shown in Figure 2 (b). For these tests, Ag/CNT composites with a CNT concentration of 4 wt. % were used as the conductive material. The resistance of the Ag/CNT composite circuit on the MC substrate increased when stress was applied. Under a strain of 0.08 mm/mm, the electrical performance (R/R_0) of the circuits on the MC substrates with various thicknesses was stable. However, from a strain of 0.08 mm/mm onwards, the resistance ratio (R/R_0) increased with the thickness of the MC substrate. At a strain of 0.266 mm/mm, the resistance ratio for the 100 μm substrate was 4.12, whereas that for the 300 μm substrate was 8.93.

Dielectric constant of MC substrate

We evaluated the dielectric constants of the MC substrates. Figure 4 (a) shows a diagram of the measurement procedure for the capacitances. The MC substrates of various thicknesses (from 100 μm to 300 μm) were placed between 50 × 50 mm aluminum plates, and their capacitances were measured at 1 kHz and DC bias conditions using an LCR meter (Grove et al. 2005). The dielectric constants were calculated from the capacitances according to (2) (Tao et al. 2020).

$$\varepsilon_\gamma = \frac{C \times d}{A \times \varepsilon_0} \qquad (2)$$

where C is the capacitance, ε_0 is the dielectric constant of vacuum ($\varepsilon_0 = 8.854 \times 10^{-12}$ Fm^{-1}), A is the area of the electrodes, and d is thickness of the MC substrate. Figure 4 (b) shows a graph of the capacitances and dielectric constants with respect to the thicknesses of the MC substrates. The average dielectric constant of the substrates was approximately 2.87, with a minimum value of 2.81 (150 μm thickness) and maximum of 3.12 (200 μm thickness) owing to the surface uniformity and non-uniform thickness caused by the evaporation process. However, majority of the dielectric constant values were stable with thickness.

Mechanical test for MC FPCB

The substrates and circuits of MC FPCBs exhibit flexibility. To improve the mechanical properties and electrical conductivity of the composite circuits, CNTs were mixed in the composites. Ag/CNT composite circuits provide mechanical endurance toward bending and torsional stresses. To determine the best electrical performance with mechanical bending and torsion, Ag/CNT composite circuits with various CNT concentrations were investigated via various methods as shown in Figure 5. Composites with four different CNT concentrations (0 wt. %, 4.3 wt. %, 9.9 wt. %, and 16.7 wt. %) were deposited onto the MC substrates in a 2 × 2 inch area. Figure S3 shows the images of the composites with four different CNT concentrations layered onto the MC substrates. Figure 5 (b) shows the SEM images of the A composites layered onto the substrates. Figures 5 (b) (□-□) show the SEM images of the composite with the highest CNT concentration (16.7 wt. %). The morphology of the composite with a CNT concentration of 16.7 wt. % was larger than that of the other composites, which means that higher the concentration of the CNTs the higher the degree of particle bonding. We analyzed the I-V curves of the composites with four different CNT concentrations (Figure 5(c)). The curves showed linear and symmetric current flow from -1.1 V to 1.1 V. The slope of the curves increased with the CNT concentration owing to the higher resistance of CNT than that of Ag. In addition, we tested the resistance ratio (R/R0) with respect to mechanical stresses such as bending and torsional stresses (Figure 5(e)). The resistances of majority of the composites were stable during bending and torsion. However, during the bending test the resistance ratio of the composite with the 4.3 wt. % of CNTs was 1.02, whereas that of the composite with 16.7 wt. % of CNTs was 1.82 (green dot in Figure 5(d)). Furthermore, during the torsional test the resistance ratio of the composite with 4.3 wt. % of CNTs was 1.04, whereas that of the composite with 16.7 wt. % of CNTs was 2.36 (green dot in Figure 5 (e)). The resistance ratio, which increased by a factor of 4 for the composite with 16.7 wt. % of CNTs, indicated that the composites with 4.3 wt. % of CNTs provided a higher electrical performance.

LED circuits

Using the Ag/CNT composites, we fabricated SMD LED circuits on the MC substrates. A diagram of the fabrication process is shown in Figure 6 (a). The Ag/CNT composites were deposited with a 500 μm linewidth circuit pattern onto the MC substrates through the PET shadow mask, which was created using a laser cutter. The SMD LEDs were implanted on the circuit pattern. Then, the LED circuits were dried at

room temperature for 0.5 h to completely evaporate the IPA from the Ag/CNT composites. Figure 6 (b) shows the LED circuit that was operated at 2.5 V to switch on and off. It shows three LEDs configured in parallel in the circuit operated under similar conditions of LED light intensity and current flow. Figures 6 (c-f) show the optical microscopy images of the LED circuit that was deposited on the MC substrate.

The Ag/CNT circuitry, which had a thickness of approximately 50 μm because of the PET mask thickness, was deposited on the surface. The Ag/CNT composite circuit pattern was spread out compared to that of the design in the circuitry pattern process. The circuit was strongly bound to the surface of the MC substrate owing to the IPA suspension. In addition, the circuitry was in good contact with the contact pads of the SMD LEDs as shown in Figure 6 (e). The surfaces of the Ag/CNT composites circuitry were clearly observed in the SEM images as shown in Figures 6 (g-j). Despite the low clarity of the circuit line due to the shadow masking, it was observed that the 500 μm linewidth of the circuit was well patterned onto the MC substrate.

Single layer 5 x 5 LED display

Ag/CNT composite circuits with complex patterns could be deposited on the MC substrates. We fabricated a 5 × 5 LED display on the MC substrate using the PET shadow mask process (Figure 7 (a)). A thicker size of the composite was deposited on both ends of the LEDs to increase the contact between the LEDs and circuits. After the fabrication of the 5 × 5 LED display onto the MC substrate (Figure 7 (b)), the LED display was connected to the Arduino Mega board, which could directly control the 25 LEDs using a programming language. Each LED was operated individually using the Arduino board. To demonstrate the control of individual LEDs, we displayed the letters M and C as shown in figures 7 (c) and (d).

Wearable touch sensor array panel

For the application of the transparent and flexible properties of the MC substrates, we demonstrated the operation of a wearable touch sensor array, which had a 5 × 5 capacitance sensor. Figure 8 (a) shows a diagram of a 5 × 5 touch sensor composed of two layers of substrates. The bottom substrate had an Ag/CNT composite capacitance sensor with wiring circuits. The top substrate was the protection layer for the wiring circuits and was open to the sensors by via holes. The two substrates were assembled using DMSO. The individual touch sensor in the array showed a capacitance of approximately 3.31 pF when touched with the index finger as shown in Figure S5. For multi-touch sensing, the Arduino Mega board was used as the 5 × 5 capacitance sensor. In addition, to monitor touch sensing in real time, we developed a customized monitoring program. Figure 8 (b) shows a diagram of the touch monitoring system. The input data of the touch sensor received by the Arduino board were transmitted by the customized monitoring program on a computer (the MFC display). Figure 8 (c) shows the operation of the touch sensor. The touched array position was displayed on the customized monitoring program by highlighting the position with a green marker (for more details, the codes are shown in Figure S6). Figure 8 (d) shows the operation of the wearable on the wrist of a hand. Its operation was demonstrated by touching the area of the wearable to display the letter C on the customized monitoring program.

Via holes for multilayer MC substrates

Multilayer circuits are being used for advanced circuits and applications. The bottom and top layers are connected using via holes to increase the circuit density and design complex circuits. The top MC substrate layer with a via hole and the bottom MC substrate layer were assembled using DMSO, which was similar to the fabrication of the wearable touch sensor array. An LED was implanted on the Ag/CNT circuit of the top layer. Finally, the Ag/CNT composite was deposited at the via hole to connect the two layers. Figures 9 (a) and (b) show a diagram of a multilayer LED circuit and an image of the circuit, respectively. Figure 9 (c) shows a SEM image of the via hole for the multilayer MC substrate. The Ag/CNT composite circuits were patterned onto a double-layer MC substrate. The top and bottom layers were connected by the Ag/CNT composite through a 500 μm diameter via hole as shown in figure 9 (e). Figures 9 (d) and (f) show the SEM images of the cross-sections of the two layers. Additional images are provided in Figure S7.

Multilayer 5 x 5 LED display

Using the via hole structure, we fabricated a multilayer 5 × 5 LED display, which consisted of a 5 × 5 passive matrix array display. Figures 10 (a) and (b) show a diagram and the image of the top and bottom substrates of the multilayer 5 × 5 LED display, respectively. For the control of the LEDs, the five rows of the circuit lines on the bottom layer were connected to the Arduino digital ports. In addition, the five columns of the circuit lines were placed on the top layer, and the LEDs were selected using the Arduino digital ports. After the LEDs were assembled on the two MC substrates, they were operated by the Arduino Mega board, which communicated with the computer using a custom software as shown in figures 10 (e-g). The Arduino board received the data and operated the LED display in the right position (row lines/column lines). For more details, the codes are shown in Figure S8. To show the LED pattern, the 5 × 5 LEDs were repeatedly activated using the Arduino board by applying 2.5 V at 20 Hz. Although the operation process of a two-layer LED display is more complex (Kang et al. 2017) than that of a single layer one, which applies an individual voltage, the two-layer 5 × 5 LED display has a simpler circuit. Figure 10 (h) shows the transparency of the 5 × 5 LED display using multilayer MC substrates for the LED operation.

Communications for the cellulose devices

Finally, we demonstrated the operation of a real-time communication system for a wearable touch panel and a 5 × 5 LED display using two Arduino modules and an MFC program as shown in Figure 11 (a). The data of the touch pattern was recognized by the wearable touch panel and transmitted to the customized pattern generation program in real time through the receiver (RX) Arduino board. The pattern generation program transmitted the data to the transmission (TX) Arduino board to create the pattern on the 5 × 5 LED display. Figure 11 (b) shows a single position of the array display based on the data received from the touch panel. Figure 11 (c) shows the LED pattern created from the data received for multiple positions. The LEDs of the 5 × 5 display were scanned at 20 Hz. Figure 11 (d) shows the pattern of the letter X recognized by the touch panel after several touch actions. Subsequently, the letter X was created

on the LED display as shown in Figure 11 (e). Circuits made of cellulose-based substrates with conductive composites were fabricated for their use in wearable communication devices such as touch panels and LED displays.

Conclusion

In addition to unique properties, such as flexibility, recyclability, high dielectric constant, and light weight, eco-friendly and renewable electronics based on cellulose provide a novel field of academic research and commercial interest (Pandey et al. 2012; Pang et al. 2021). Because of their excellent recyclability and transparency, cellulose-based substrates can host more types of electronics than conventional FPCBs that are not environmentally friendly, although the process of creating a cellulose-based substrate can be extremely challenging. Here, we reported FPCBs consisting of transparent and flexible cellulose-based substrates fabricated by a simple evaporation process. Ag/CNT composites were used for the circuits, which were patterned onto the cellulose-based substrates using a shadow mask. The electrical and mechanical properties of the MC substrate-based FPCBs were observed under diverse mechanical stresses such as bending, torsional, and tensile stresses. Excellent dielectric properties were observed using the capacitance measurements. In addition, the morphology of the MC substrate circuits were analyzed using optical microscopy, SEM, and XRD. To demonstrate the application of the FPCBs, we fabricated a 5 × 5 touch panel that successfully controlled a 5 × 5 LED display, which was fabricated using MC FPCBs as well.

Although the Ag/CNT line pattern on the MC substrates was not fine because of the PET shadow mask, we demonstrated the operation of wearable communication devices controlled by a computer. In this study, we reported only a few applications including the control of an SMD LED display device by human–machine interfaces (Ferreira et al. 2008; Riviere and Thakor 1996). Eco-friendly and nontoxic cellulose-based flexible devices can be used in diverse applications such as paper robots (Shigemune et al. 2017; Mazzeo et al. 2021), wearable devices (Noh and Song 2020a, b), transparent advanced circuits (Song et al. 2017; Noh et al. 2021), and embedded electronics (Kim et al. 2018; Nandy et al. 2021). Furthermore, MC substrates can be used for electrochemical applications such as DNA control (Song et al. 2018; Lee et al. 2021; Song et al. 2020) and protein detection (Berggård et al. 2007).

Declarations

Funding

This work was supported by the National Research Foundation of Korea (NRF) grant funded by the Korean government (NRF- 2021R1F1A1061052 and NRF- 2021R1A4A3031992).

References

1. STECKL, Andrew J (2013) Circuits on cellulose. IEEE Spectrum 50.2: 48-61. https://doi.org/10.1109/MSPEC.2013.6420146
2. Alimenti F, Mariotti C, Palazzi V, Virili M, Orecchini G, Mezzanotte P, Roselli L (2015) Communication and sensing circuits on cellulose. Journal of Low Power Electronics and Applications 5.3: 151-164. https://doi.org/10.3390/jlpea5030151
3. Jung YH, Chang TH, Zhang H, Yao C, Zheng Q, Yang VW, Mi HY, Kim MH, Cho SJ, Park DW, Jiang H, Lee JH, Qiu Y, Zhou W, Cai Z, Gong S, Ma Z (2015) High-performance green flexible electronics based on biodegradable cellulose nanofibril paper. Nature communications 6.1: 1-11. https://doi.org/10.1038/ncomms8170
4. Shin SR., Farzad R, Tamayol A, Manoharan V, Mostafalu P, Zhang YS, Akbari M, Jung SM, Kim DJ, Comotto M, Annabi N, Al-hazmi FE, Dokmeci MR, Khademhosseini A (2016) A bioactive carbon nanotube-based ink for printing 2D and 3D flexible electronics. Advanced Materials 28.17: 3280-3289. https://doi.org/10.1002/adma.201506420
5. Lin Y, Gritsenko D, Liu Q, Lu X, Xu J (2016) Recent advancements in functionalized paper-based electronics. ACS applied materials & interfaces 8.32: 20501-20515. https://doi.org/10.1021/acsami.6b04854
6. Ko Y, Kwon M, Bae WK, Lee B, Lee, SW, Cho J (2017) Flexible supercapacitor electrodes based on real metal-like cellulose papers. *Nature communications* 8.1: 1-11. https://doi.org/10.1038/s41467-017-00550-3
7. Jabbour L, Bongiovanni R, Chaussy D, Gerbaldi C, Beneventi, D (2013) Cellulose-based Li-ion batteries: a review. Cellulose 20.4: 1523-1545. https://doi.org/10.1007/s10570-013-9973-8
8. Guan X, Hou Z, Wu K, Zhao H, Liu S, Fei T, Zhang T (2021) Flexible humidity sensor based on modified cellulose paper. Sensors and Actuators B: Chemical 339: 129879. https://doi.org/10.1016/j.snb.2021.129879
9. Wang HK, Tsai CH, Chen KH, Tang CT, Leou JS, Li PC, Tang YL, Hsieh HJ, Wu HC, Cheng CM (2014) Cellulose-based diagnostic devices for diagnosing Serotype-2 dengue fever in human serum. Advanced healthcare materials 3.2: 187-196. https://doi.org/10.1002/adhm.201300150
10. Shin S, Hyun J (2017) Matrix-assisted three-dimensional printing of cellulose nanofibers for paper microfluidics. ACS applied materials & interfaces 9.31: 26438-26446. https://doi.org/10.1021/acsami.7b07609
11. Fujisaki Y, Koga H, Nakajima Y, Nakata M, Tsuji H, Yamamoto T, Nogi M, Shimidzu N (2014) Transparent nanopaper-based flexible organic thin-film transistor array. Advanced Functional Materials 24.12: 1657-1663. https://doi.org/10.1002/adfm.201303024
12. Nogi M, Iwamoto S, Nakagaito AN, Yano H (2009) Optically transparent nanofiber paper. Advanced materials 21.16: 1595-1598. https://doi.org/10.1002/adma.200803174
13. Wang Q, Cai J, Zhang L, Xu M, Cheng H, Han CC, Kuga S, Xiao J, Xiao R (2013) A bioplastic with high strength constructed from a cellulose hydrogel by changing the aggregated structure. Journal of Materials Chemistry A 1.22: 6678-6686. https://doi.org/10.1039/C3TA11130J

14. Song Y, Kim S, Heller MJ (2017) An implantable transparent conductive film with water resistance and ultrabendability for electronic devices. ACS applied materials & interfaces 9.48: 42302-42312. https://doi.org/10.1021/acsami.7b11801
15. Noh S, An H, Song Y (2021) Vacuum-filtration fabrication for diverse conductive transparent cellulose electronic devices. Cellulose 28.5: 3081-3096. https://doi.org/10.1007/s10570-021-03708-x
16. Koga H, Nogi M, Komoda N, Nge TT, Sugahara T, Suganuma K (2014) Uniformly connected conductive networks on cellulose nanofiber paper for transparent paper electronics. NPG Asia Materials 6.3: e93-e93. https://doi.org/10.1038/am.2014.9
17. Ebner M, Schennach R, Chien HT, Mayrhofer C, Zankel A, Friedel B (2017) Regenerated cellulose fiber solar cell. Flexible and Printed Electronics 2.1: 014002. https://doi.org/10.1088/2058-8585/aa5707
18. Dai S, Chu Y, Liu D, Cao F, Wu X, Zhou J, Zhou B, Chen Y, Huang J (2018) Intrinsically ionic conductive cellulose nanopapers applied as all solid dielectrics for low voltage organic transistors. Nature communications 9.1: 1-10. https://doi.org/10.1038/s41467-018-05155-y
19. Nair KG, Jayaseelan D, Biji P (2015) Direct-writing of circuit interconnects on cellulose paper using ultra-long, silver nanowires based conducting ink. RSC advances 5.93: 76092-76100. https://doi.org/10.1039/C5RA10837C
20. Han JW, Kim B, Li J (2014) Carbon nanotube ink for writing on cellulose paper. Materials Research Bulletin 50: 249-253. https://doi.org/10.1016/j.materresbull.2013.10.048
21. Ham J, Dong WJ, Jung GH, Lee JL (2016) Wavelength-scale structures as extremely high haze films for efficient polymer solar cells. ACS applied materials & interfaces 8.9: 5990-5997. https://doi.org/10.1021/acsami.5b11061
22. Nagashima K, Koga H, Celano U, Zhuge F, Kanai M, Rahong S, Meng G, He Y, Boeck JD, Jurczak M, Vandervorst W, Kitaoka T, Nogi M, Yanagida T (2014) Cellulose nanofiber paper as an ultra flexible nonvolatile memory. Scientific reports 4.1: 1-7. https://doi.org/10.1038/srep05532
23. Park CB, Kim KM, Lee JE, Na H, Yoo SS, Yang MS (2014) Flexible electrophoretic display driven by solution-processed organic TFT with highly stable bending feature. Organic Electronics 15.12: 3538-3545. https://doi.org/10.1016/j.orgel.2014.09.039
24. Son D, Lee J, Qiao S, Ghaffari R, Kim J, Lee JE, Song CY, Kim SJ, Lee DJ, Jun SW, Yang SX, Park MJ, Shin JH, Do KS, Lee MC, Kang KH, Hwang CS, Lu NS, Hyeon TG, Kim DH (2014) Multifunctional wearable devices for diagnosis and therapy of movement disorders. Nature nanotechnology 9.5: 397. https://doi.org/10.1038/nnano.2014.38
25. Kamiya S, Furuta H, Omiya M (2007) Adhesion energy of Cu/polyimide interface in flexible printed circuits. Surface and Coatings Technology 202.4-7: 1084-1088. https://doi.org/10.1016/j.surfcoat.2007.07.061
26. Kim HL, Kim YH, Kim YJ (2008) Miniature electrocardiography sensor using a flexible printed circuit and MEMS technology. In: 2008 IEEE International Conference on Multisensor Fusion and Integration for Intelligent Systems IEEE p. 545-550. https://doi.org/10.1109/MFI.2008.4648052

27. Yeon SH, Shu T, Rogers EA, Song H, Hsieh TH, Freed LE, Herr HM (2020) Flexible Dry Electrodes for EMG Acquisition within Lower Extremity Prosthetic Sockets. In: 2020 8th IEEE RAS/EMBS International Conference for Biomedical Robotics and Biomechatronics (BioRob) IEEE p. 1088-1095. https://doi.org/10.1109/BioRob49111.2020.9224338
28. Lee C, Kim M, Kim YJ, Hong N, Ryu S, Kim HJ, Kim S (2017) Soft robot review. International Journal of Control, Automation and Systems 15.1: 3-15. https://doi.org/10.1007/s12555-016-0462-3
29. Chu JH, Joo SJ, Kim HS (2019) Development of a via-hole connection process via intense pulsed light sintering with Cu micro/Ag nano-hybrid ink for a multi-layered flexible printed circuit board. Thin Solid Films 680: 1-11. https://doi.org/10.1016/j.tsf.2019.04.015
30. Lee JS, Kang SJ, Shin JH, Shin YJ, Lee B, Koo JM, Kim TI (2020) Nanoscale-Dewetting-Based Direct Interconnection of Microelectronics for a Deterministic Assembly of Transfer Printing. Advanced Materials 32.21: 1908422. https://doi.org/10.1002/adma.201908422
31. Kim J, Song CS, Yun SR (2006) Cellulose based electro-active papers: performance and environmental effects. Smart Materials and Structures 15.3: 719. https://doi.org/10.1088/0964-1726/15/3/007
32. Gustafsson C, Bonferoni MC, Caramella C, Lennholm H, Nyström C (1999) Characterisation of particle properties and compaction behaviour of hydroxypropyl methylcellulose with different degrees of methoxy/hydroxypropyl substitution. European journal of pharmaceutical sciences 9.2: 171-184. https://doi.org/10.1016/S0928-0987(99)00054-8
33. Yu, Denis YW, Frans Spaepen (2004) The yield strength of thin copper films on Kapton. Journal of Applied Physics 95.6: 2991-2997. https://doi.org/10.1063/1.1644634
34. Kumar K, Pooleery A, Madhusoodanan K, Singh RN, Chatterjee A, Dutta BK, Sinha RK (2016) Optimisation of thickness of miniature tensile specimens for evaluation of mechanical properties. Materials Science and Engineering: A 675: 32-43. https://doi.org/10.1016/j.msea.2016.08.032
35. Lim H, Hoag SW (2013) Plasticizer effects on physical–mechanical properties of solvent cast Soluplus® films. Aaps Pharmscitech 14.3: 903-910. https://doi.org/10.1208/s12249-013-9971-z
36. McKenna BA, Mikkelsen D, Wehr JB, Gidley MJ, Menzies NW (2009) Mechanical and structural properties of native and alkali-treated bacterial cellulose produced by Gluconacetobacter xylinus strain ATCC 53524. Cellulose 16.6: 1047-1055. https://doi.org/10.1007/s10570-009-9340-y
37. Grove TT, Masters MF, Miers RE (2005) Determining dielectric constants using a parallel plate capacitor. American journal of physics 73.1: 52-56. https://doi.org/10.1119/1.1794757
38. Tao J, Cao SA. Shun-an (2020) Flexible high dielectric thin films based on cellulose nanofibrils and acid oxidized multi-walled carbon nanotubes. RSC Advances 10.18: 10799-10805. https://doi.org/10.1039/C9RA10915C
39. Kang CM, Kong DJ, Shim JP, Kim S, Choi SB, Lee JY, Jung HM, Seo DJ, Choi SY, Lee DS (2017) Fabrication of a vertically-stacked passive-matrix micro-LED array structure for a dual color display. Optics Express 25.3: 2489-2495. https://doi.org/10.1364/OE.25.002489

40. Pandey JK, Takagi H, Nakagaito AN, Saini DR, Ahn SH (2012) An overview on the cellulose based conducting composites. Composites Part B: Engineering 43.7: 2822-2826. https://doi.org/10.1016/j.compositesb.2012.04.045
41. Pang B, Jiang G, Zhou J, Zhu Y, Cheng W, Zhao D, Wang K, Xu G, Yu H (2021) Molecular-Scale Design of Cellulose-Based Functional Materials for Flexible Electronic Devices. Advanced Electronic Materials 7.2: 2000944. https://doi.org/10.1002/aelm.202000944
42. Ferreira A, Celeste WC, Cheein FA, Bastos-Filho TF, Sarcinelli-Filho M, Carelli R (2008) Human-machine interfaces based on EMG and EEG applied to robotic systems. Journal of NeuroEngineering and Rehabilitation 5.1: 1-15. https://doi.org/10.1186/1743-0003-5-10
43. Riviere CN, Thakor NV (1996) Modeling and canceling tremor in human-machine interfaces. IEEE engineering in medicine and biology magazine 15.3: 29-36. https://doi.org/10.1109/51.499755
44. Shigemune H, Maeda S, Cacucciolo V, Iwata Y, Iwase E, Hashimoto S, Sugano S (2017) Printed paper robot driven by electrostatic actuator. IEEE Robotics and Automation Letters 2.2: 1001-1007. https://doi.org/10.1109/LRA.2017.2658942
45. Mazzeo AD, Liang T, Zou X, Xie J, Ashraf A, Salvi D, Berthiaume F, Pal RK (2021) Paper as a substrate and smart material for electronics, packaging, and robotics. In: 2021 IEEE International Conference on Flexible and Printable Sensors and Systems (FLEPS) IEEE p. 1-3. https://doi.org/10.1109/FLEPS51544.2021.9469859
46. Noh S, Song Y (2020) A simple transparent electrode fabrication method by filling in Ag composites into scratch gap. Microelectronic Engineering 228: 111331. https://doi.org/10.1016/j.mee.2020.111331
47. Noh S, Song Y (2020) Elastic CNT nanocomposites for Joule heating and tactic sensing devices. Mechanics of Advanced Materials and Structures 1-9. https://doi.org/10.1080/15376494.2020.1842950
48. Kim D, Ko Y, Kwon G, Kim UJ, You J (2018) Micropatterning silver nanowire networks on cellulose nanopaper for transparent paper electronics. ACS applied materials & interfaces 10.44: 38517-38525. https://doi.org/10.1021/acsami.8b15230
49. Nandy S, Goswami S, Marques A, Gaspar D, Grey P, Cunha I, Nunes D, Pimentel A, Igreja R, Barquinha P, Pereira L, Forunato E, Martins R (2021) Cellulose: A Contribution for the Zero e-Waste Challenge. Advanced Materials Technologies 2000994. https://doi.org/10.1002/admt.202000994
50. Song Y, Kim S, Heller MJ, Huang X (2018) DNA multi-bit non-volatile memory and bit-shifting operations using addressable electrode arrays and electric field-induced hybridization. Nature communications 9.1: 1-8. https://doi.org/10.1038/s41467-017-02705-8
51. Lee W, Yu M, Lim D, Kang T, Song Y (2021) Programmable DNA-Based Boolean Logic Microfluidic Processing Unit. ACS nano 2021. https://doi.org/10.1021/acsnano.1c02153
52. Song Y, Kim S, Heller MJ (2020) A programmable macroscale electrical field self-assembly array device for diverse thin film applications. Journal of Materials Research and Technology 9.4: 8808-8819. https://doi.org/10.1016/j.jmrt.2020.06.033

53. Berggård T, Linse S, James, P (2007) Methods for the detection and analysis of protein–protein interactions. Proteomics 7.16: 2833-2842. https://doi.org/10.1002/pmic.200700131

Figures

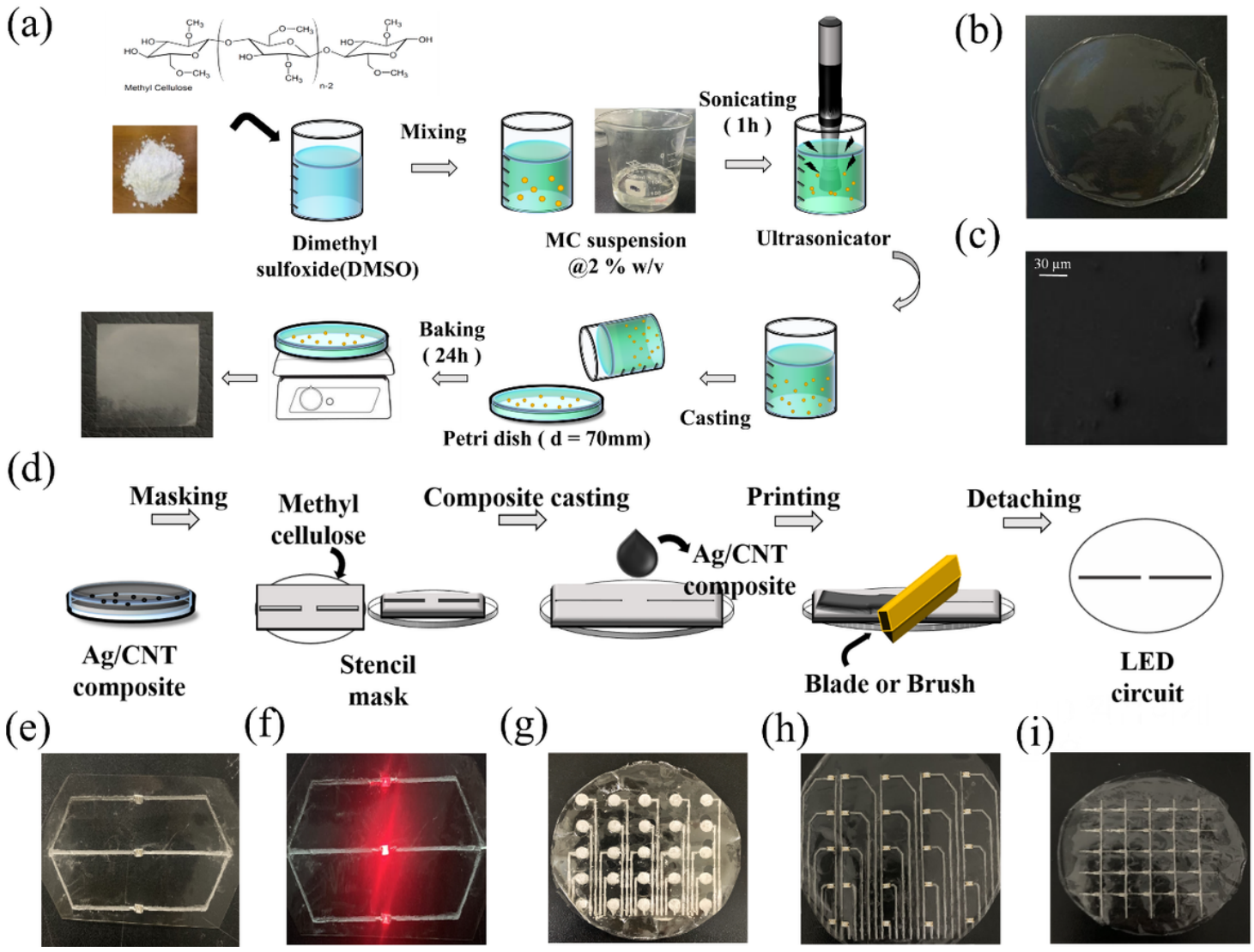

Figure 1

(a) Fabrication process for the MC substrates. (b) Image of the transparent MC substrate. (c) SEM image of the MC substrate. (d) Fabrication process for the Ag/CNT circuit. (e–f) Images of the parallel LED circuit turned (e) off and (f) on. (g–i) Images of single layer and multilayer circuits.

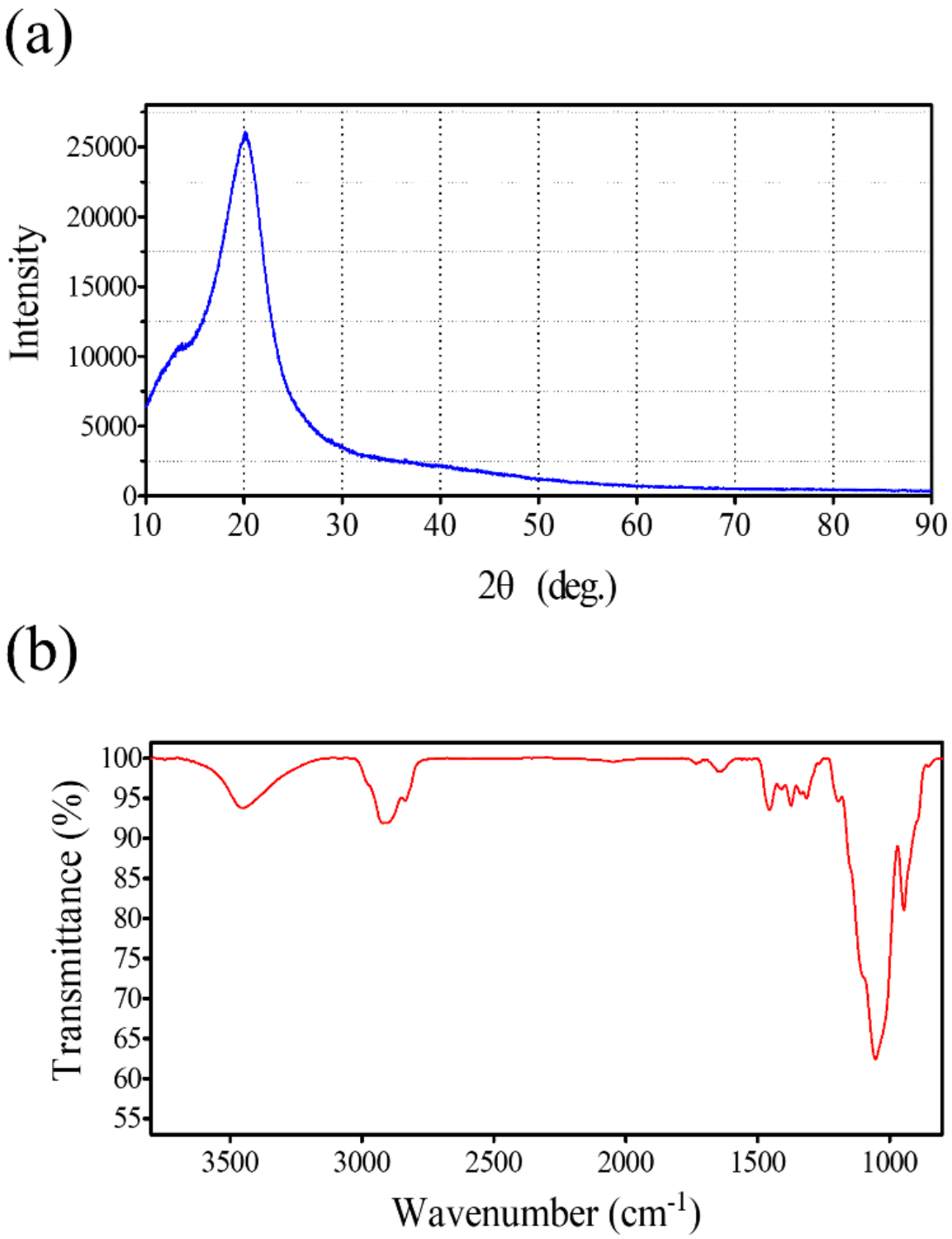

Figure 2

(a) XRD pattern and (b) FTIR spectrum of the MC substrate

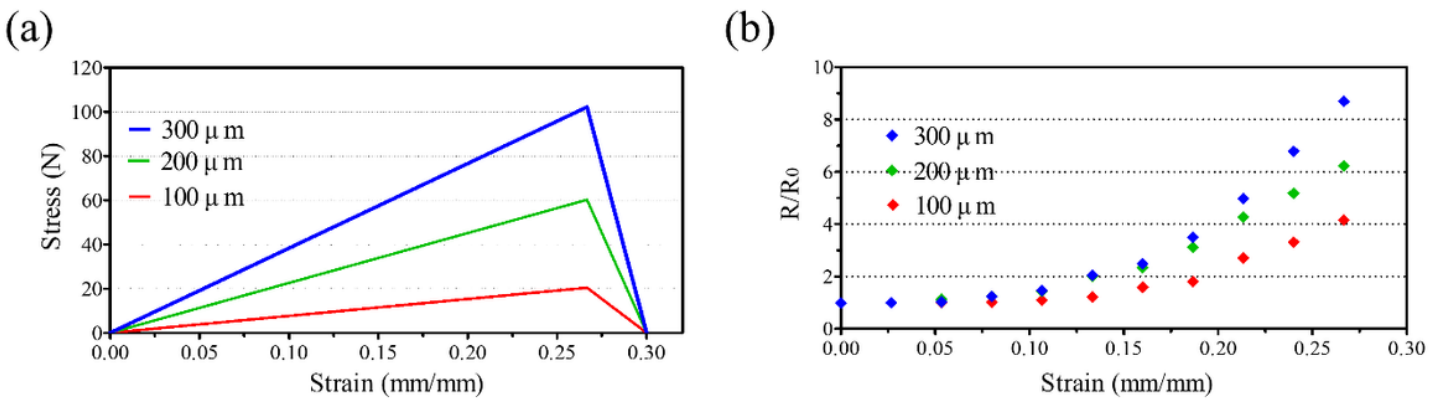

Figure 3

(a) Stress–strain curves and (b) resistance-ratio–strain curves of the MC substrates with various thicknesses.

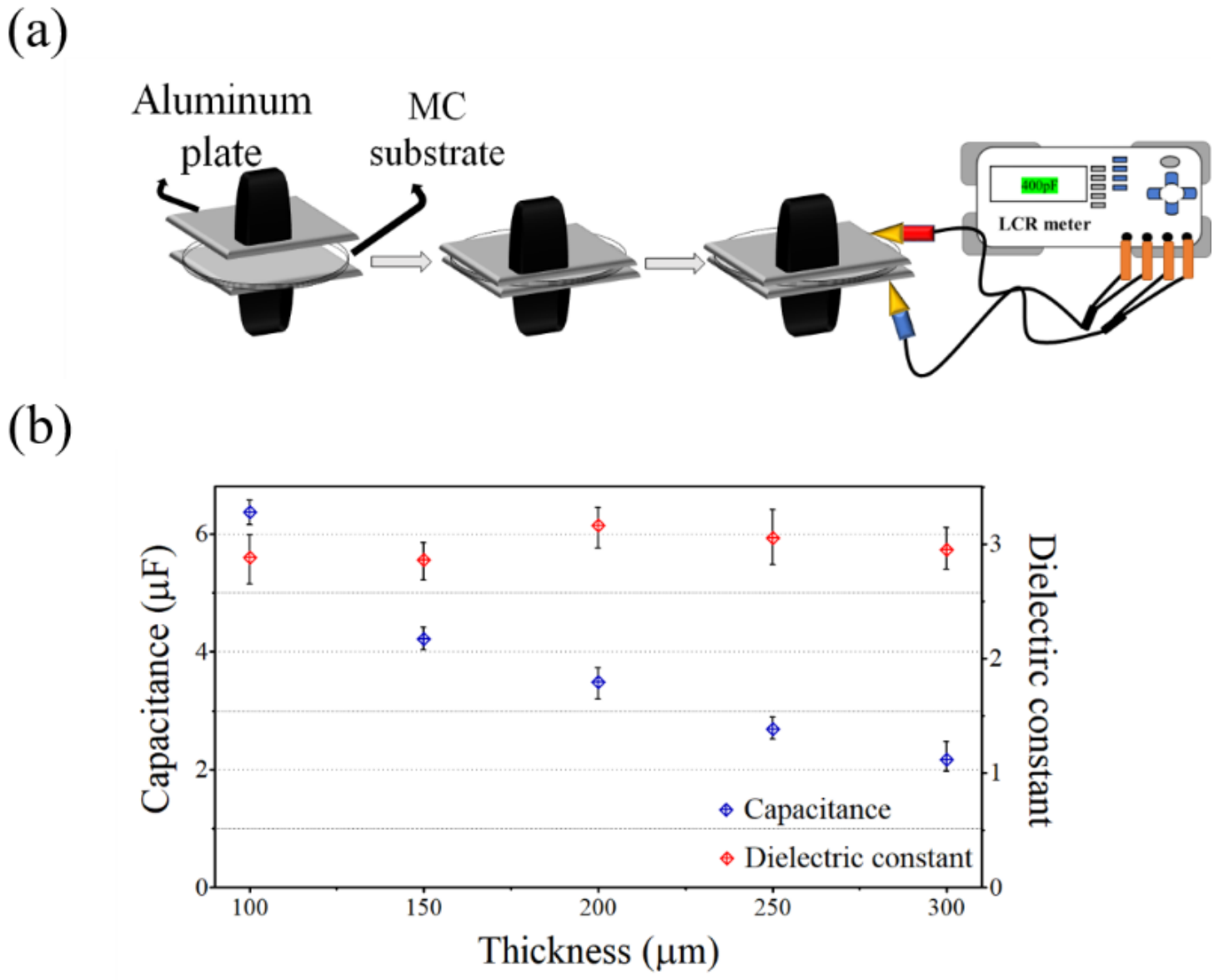

Figure 4

(a) Capacitance measurement procedure. (b) Graph of capacitance and dielectric constant with respect to the MC substrate thickness.

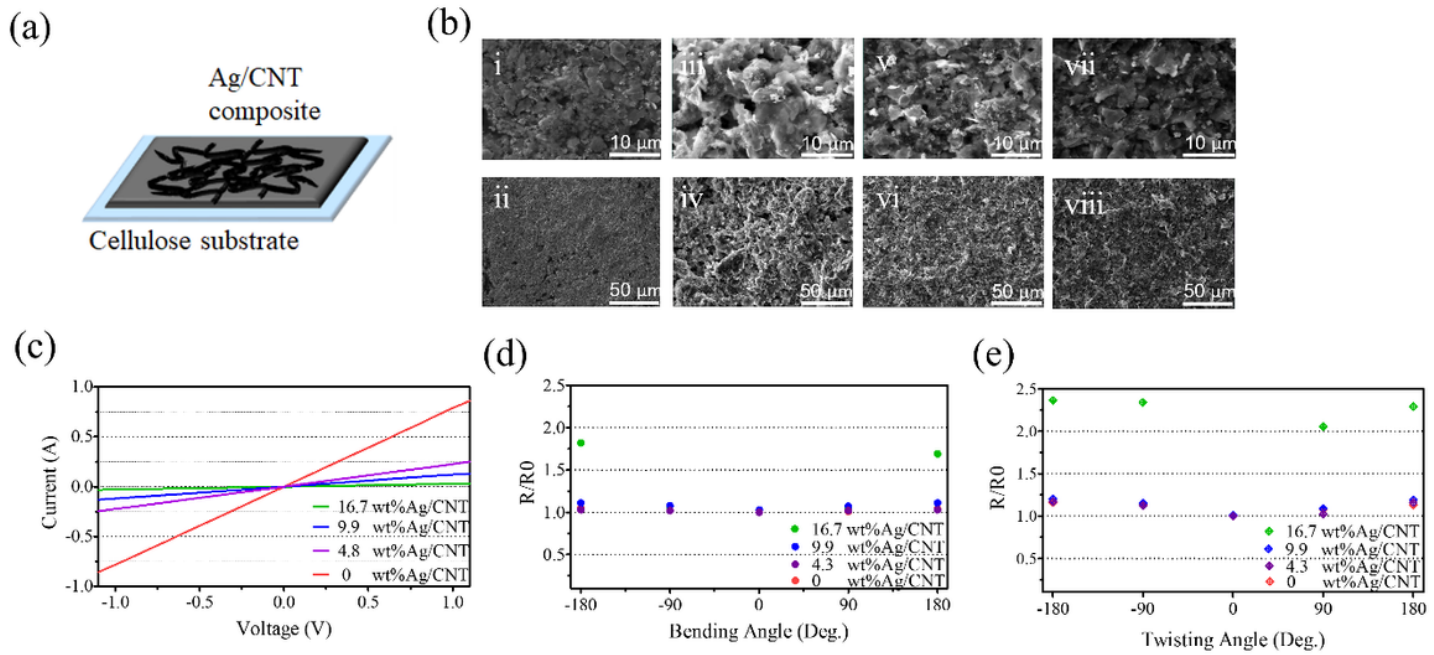

Figure 5

(a) Schematic of the Ag/CNT composite on the MC substrate. (b) SEM images of the Ag/CNT composites on the MC substrate. (c) I–V curves of Ag/CNT composite circuits. (d–e) graph of resistance ratio with respect to (d) bending angle and (e) twisting angle.

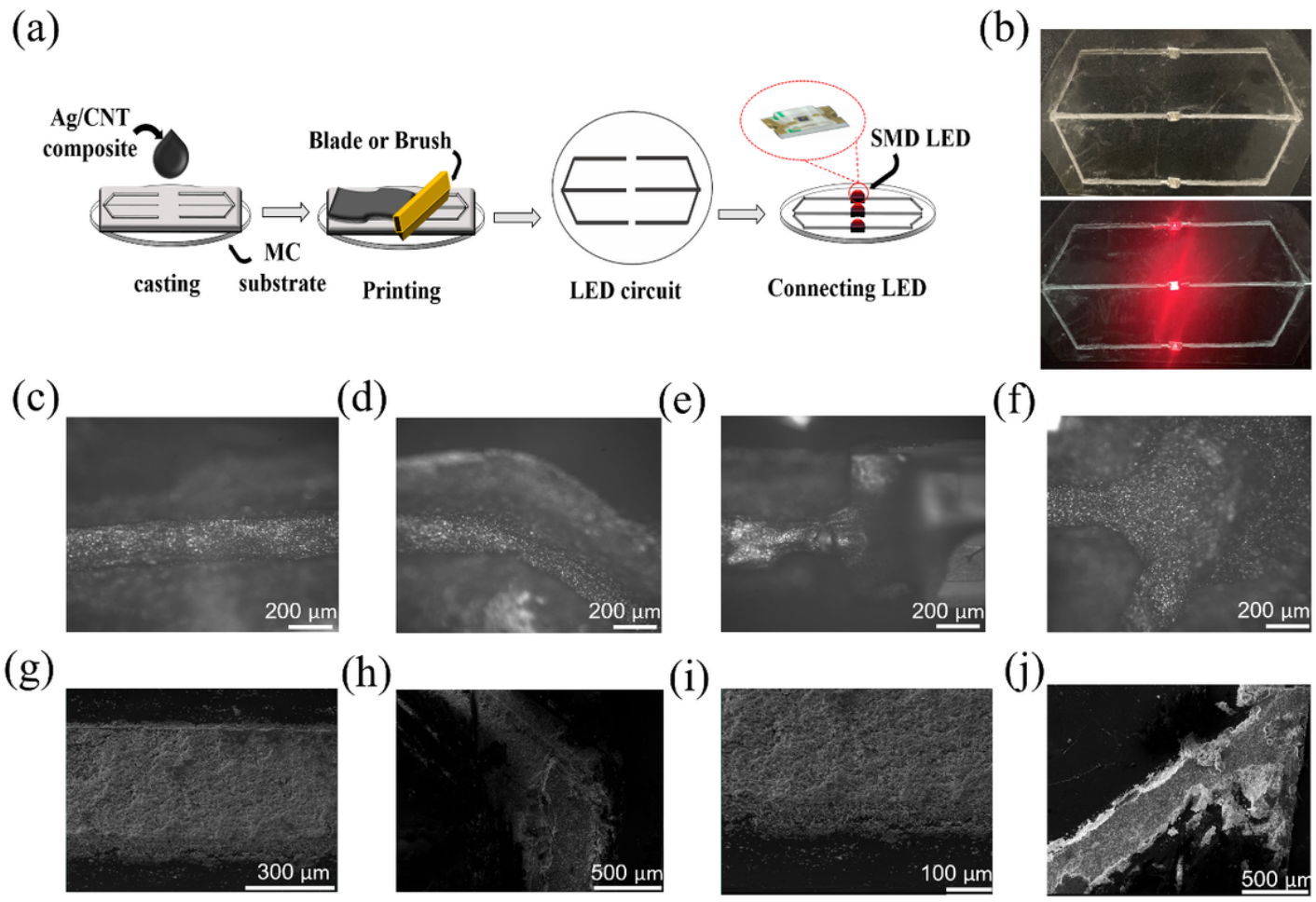

Figure 6

(a) Fabrication process of the LED circuit. (b) Images of the LED circuit. (c–f) Optical microscopy images of the LED circuits. (g–j) SEM images of the LED circuits.

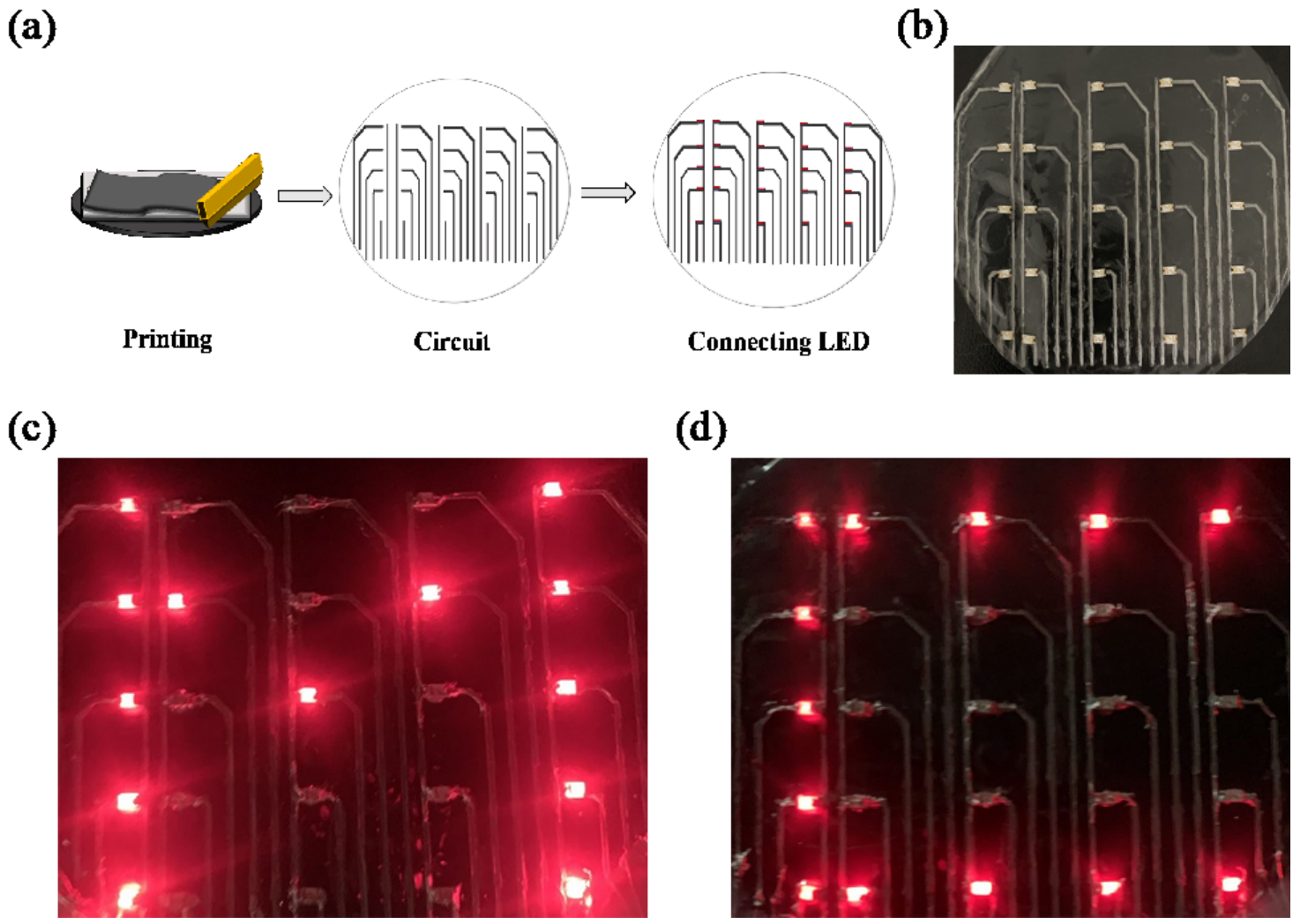

Figure 7

(a) Fabrication process of the 5 × 5 LED circuit. (b) Image of the 5 × 5 LED circuit. (c–d) Images of the operation of the LED circuit.

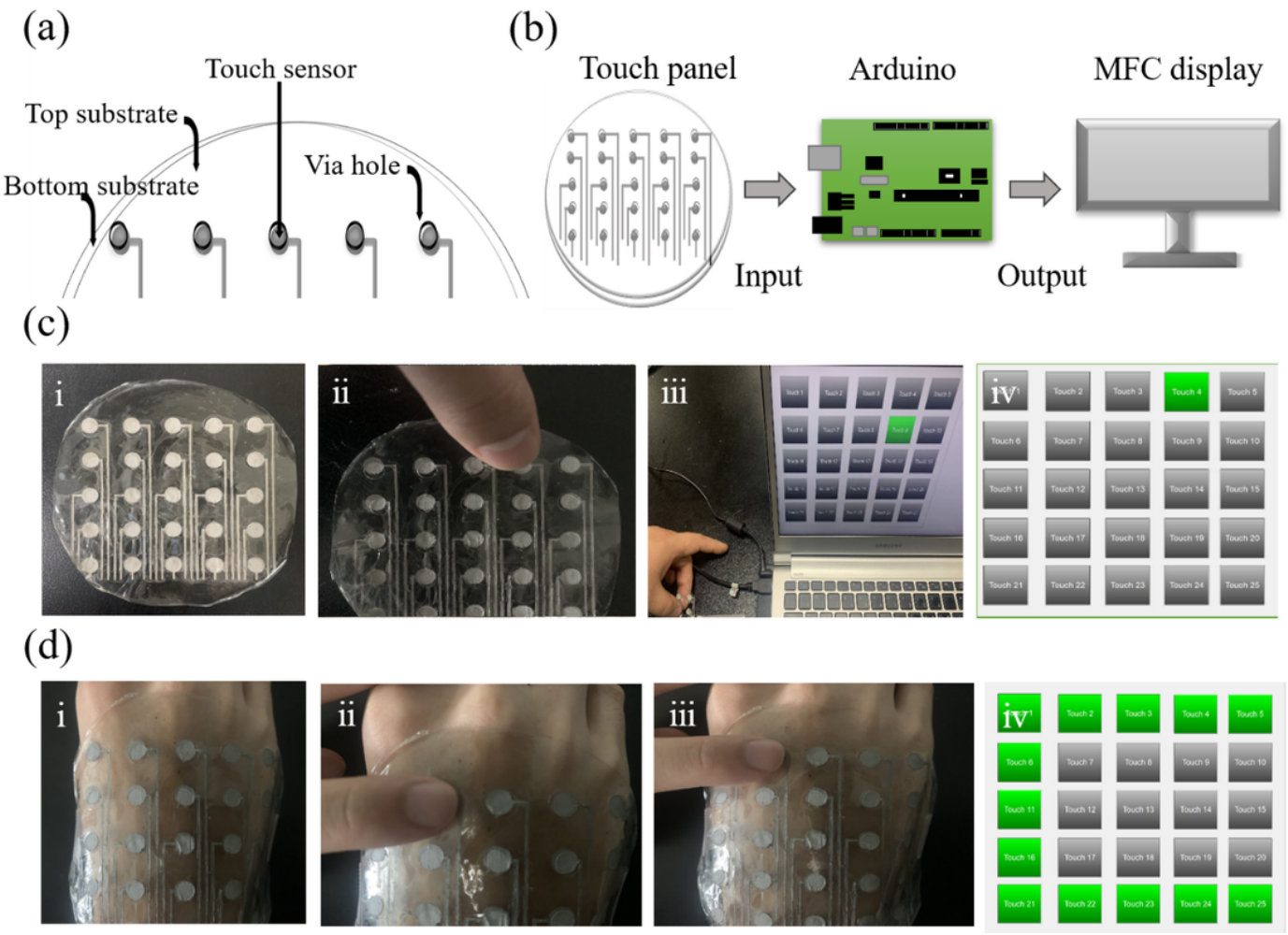

Figure 8

(a) Diagram of the multilayer touch sensor panel. (b) The communication process between the sensor, Arduino board, and MFC display. (c–d) Images of the touch operation and display.

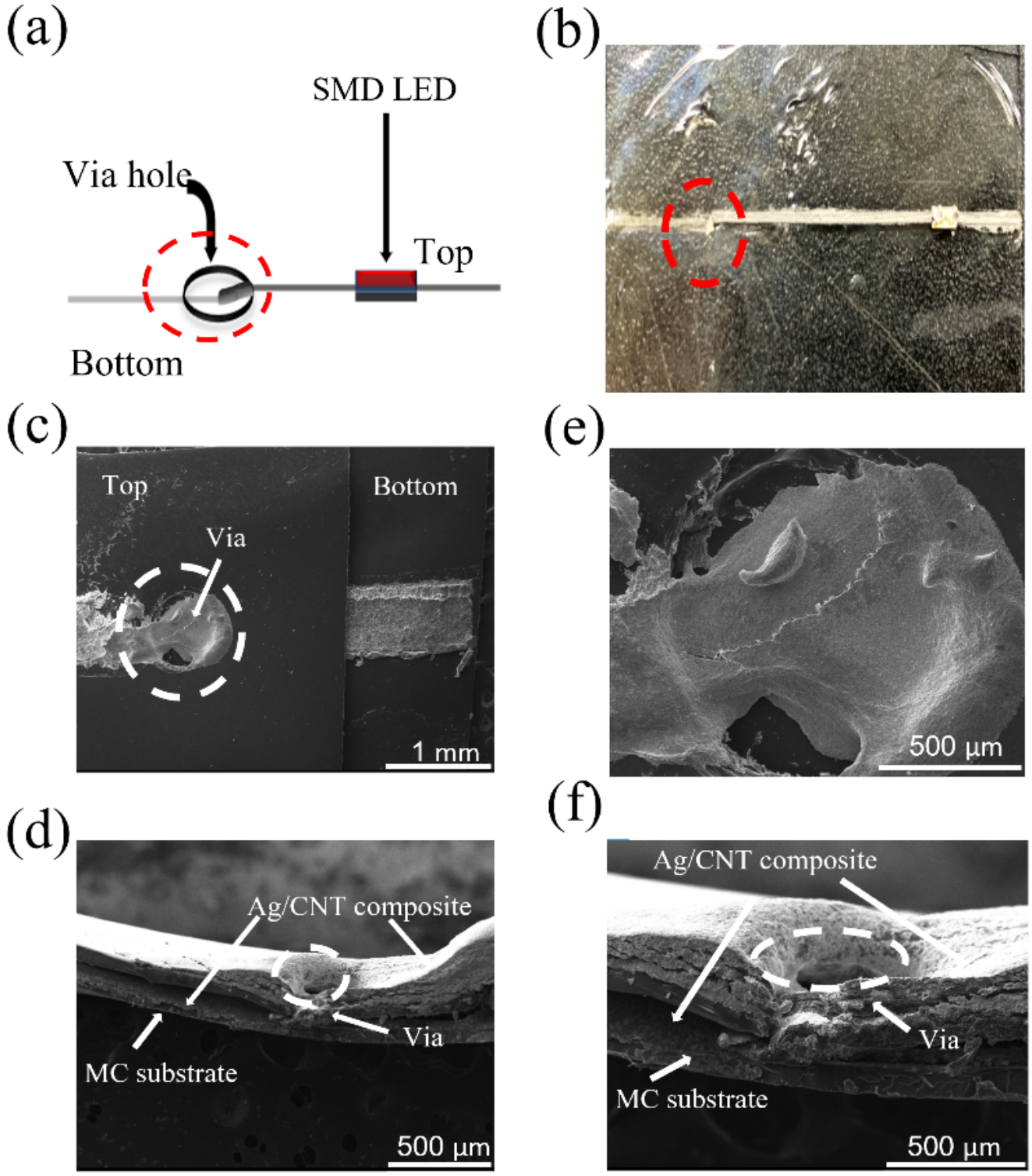

Figure 9

(a) Diagram of a multilayer LED circuit with a via hole. (b) Image of the circuit with the via hole. (c–d) SEM images and (e–f) Magnify SEM images of the multilayer circuits with the via holes in top view and side view.

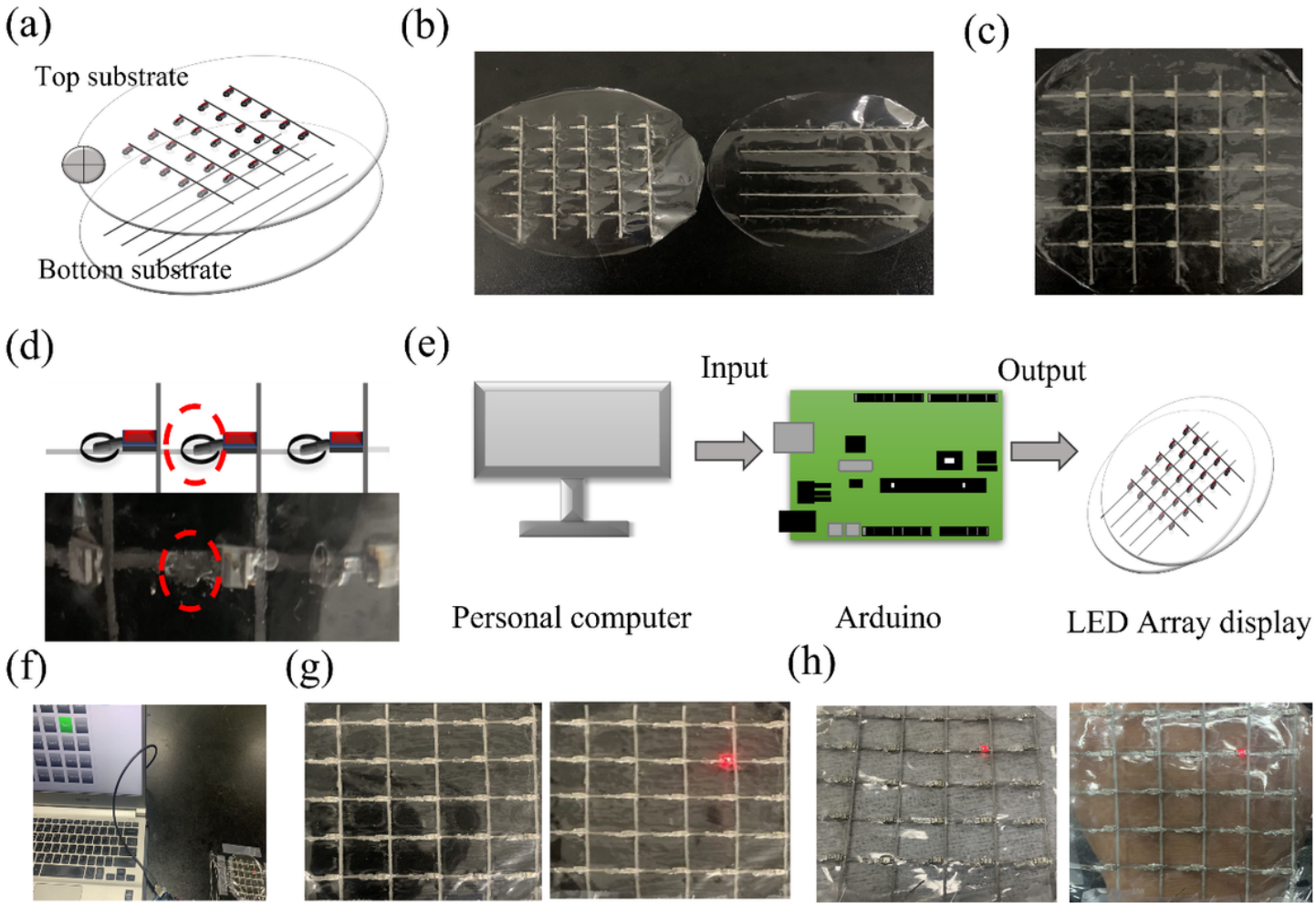

Figure 10

(a) Diagram and (b) image of the top and bottom substrates. (c) The assembled layers with LEDs. (d) Diagram and image of the via hole. (e) The communication process between the Arduino board, MFC program, and LED display (f–h) images of the operation of the LED display.

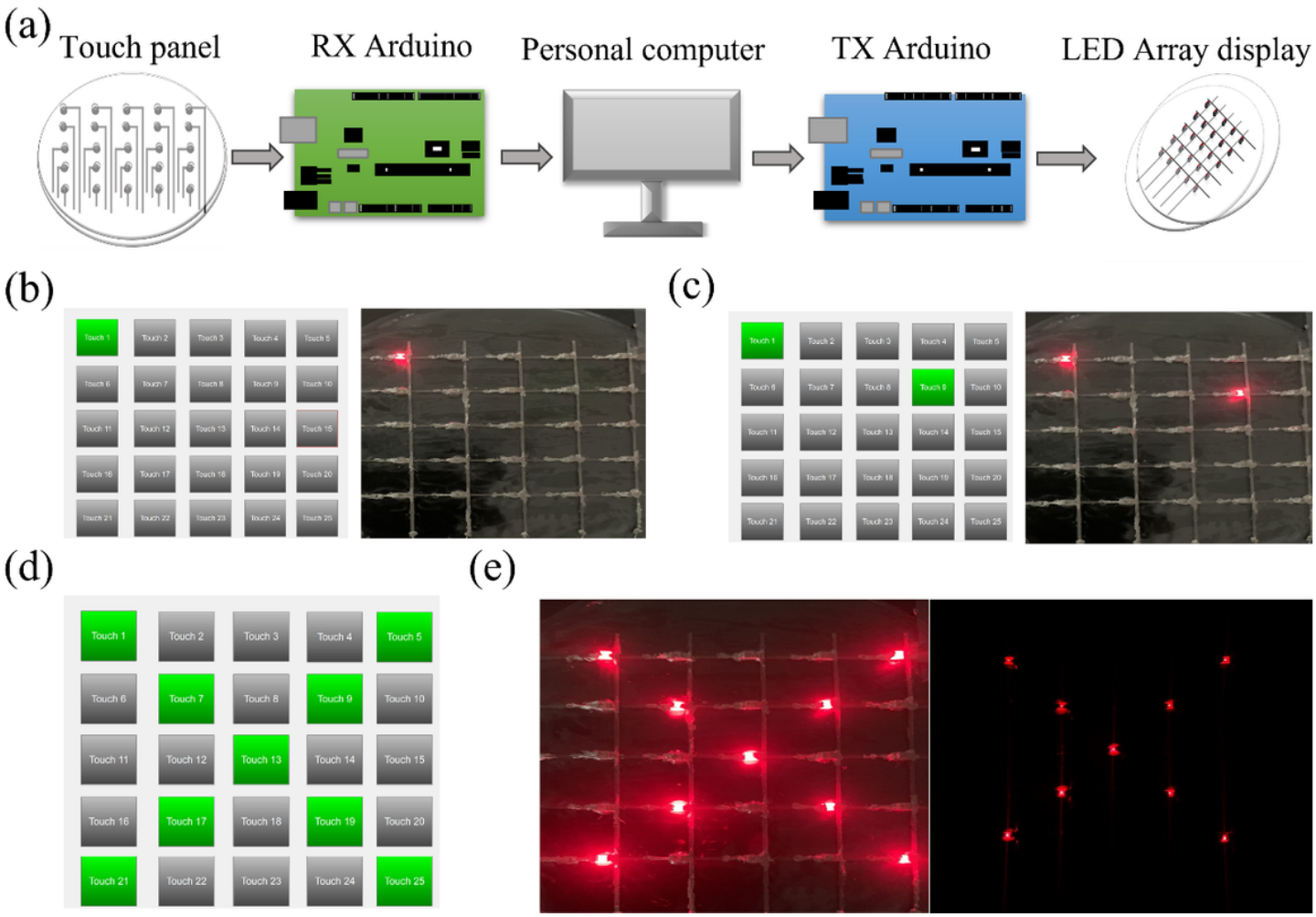

Figure 11

(a) Communication process between the multilayer circuits, MFC program, and Arduino boards. (b–e) Images of the operation of the communication system.

Supplementary Files

This is a list of supplementary files associated with this preprint. Click to download.

- SupplementaryMaterial.docx